Charge state switching of the divacancy defect in 4H-SiC

Ariana Beste, DeCarlos E. Taylor, D. Andrew Golter, and Chih W. Lai

Phys. Rev. B **98**, 214107 — Published 10 December 2018

DOI: 10.1103/PhysRevB.98.214107

Charge State Switching of the Divacancy Defect in 4H-SiC

Ariana Beste[a†], DeCarlos E. Taylor[a], D. Andrew Golter [b,c], and Chih W. Lai[b,c]

[a] *US Army Research Laboratory, Deer Creek Loop, Aberdeen Proving Ground, MD 21005-5069, USA*

[b] *US Army Research Laboratory, 2800 Powder Mill Road, Adelphi, MD 20783*

[c] *The MITRE Corporation, 202 Burlington Road, Bedford, MA 01730*

[†]Corresponding Author

ariana.beste.ctr@mail.mil

Abstract

Optical charge state switching was previously observed in photoluminescence experiments for the divacancy defect in 4H-SiC. The participating dark charge state could not be identified with certainty. We use constrained DFT to investigate the mechanism of charge state conversion from the bright neutral charge state of the divacancy defect to the positive and negative charge states including corresponding recovery of the neutral charge state. While we can confirm that the positive charge state is dark, we do not find evidence that the negative charge state is dark. We compute similar absorption energies required for conversion of the neutral defect to both charge states. However, the formation of the positive charge state requires a series of excitations involving a 2-photon excitation, while the creation of the negative charge state is achieved through a single 2-photon process. Calculated absorption energies for the recovery of the neutral defect from the positive charge state fit the experimental value better than from the negative charge state. Defect formation energies as a function of the Fermi energy show a very small Fermi energy range in which the negative charge state is most stable, while the positive charge state exhibits a wide stability range. Overall, our computational results give more support to the identification of the dark charge state as the positive over the negative charge state in the mechanism of optical charge state switching.

Keywords:

Constrained density functional theory (DFT), hybrid functional, VASP, defect formation energy, localized defect states, excitation energies, ionization pathways

1. Introduction

The development of qubit materials that form the foundation for future quantum computing and sensing devices is an area of great potential but also of considerable difficulty. A qubit is a unit of quantum information analogous to a bit, which is a unit of classical information. While a bit can only be in one of two states, a qubit can be in a superposition of quantum states, permitting a qubit to store more information than a classical bit. Qubits have been realized in a variety of materials, such as electrons floating on liquid helium [1, 2], nuclear spin states of liquids [3], spin states of quantum dots coupled to superconductors [4, 5], and rare-earth doped solids [6, 7]. A qubit needs to be individually addressable, maintaining its quantum state long enough for information processing. That requires the qubit states to be isolated from their environment to avoid interference and relaxation. Isolated atoms with well-defined quantum states are a natural choice for a qubit material and have been used in a general purpose five-qubit quantum computer [8]. However, device fabrication necessitates the use of ion-traps or optical lattices. In contrast, point defects in semiconductors and insulators such as vacancies, antisites, or substitutional defects are introduced in materials during production and can be controlled by applying various techniques [9, 10]. Point defects can exhibit similar electronic behavior to isolated atoms and have been shown to be suitable for quantum computing applications [11, 12]. Characteristic of deep defect centers is the appearance of localized defect states within the band gap. The nitrogen-vacancy (NV) in diamond is an example of a deep defect center that has been explored as a candidate qubit material [13-15]. While the electronic properties of the NV center are desirable, the production of diamond devices is difficult. Alternatively, silicon carbide (SiC) is a wide band gap semi-conductor [16] that can be grown in large single crystals. A variety of stable defects such as monovacancies, divacancies, antisites, NV centers, and defect combinations have been identified in SiC [17-19] and considered as potential qubit materials [11, 12, 20].

In this work, we focus on the neutral divacancy in 4H-SiC that has been shown to be individually addressable in the near infrared [21]. The localized triplet ground state of the divacancy can be optically spin-polarized similarly to the diamond NV center [12]. After initialization, the qubit states can be coherently manipulated with pulsed microwaves and their spin states can be read out by spin dependent measurement of the photoluminescence intensity

after electronic excitation [22]. The measured zero-phonon lines (ZPLs) correspond to the transitions between the ^{3}A ground state and the structurally relaxed ^{3}E first excited state for the four distinct neutral divacancy defects in 4H-SiC. While the neutral divacancy possesses the required electronic properties to function as a qubit material, depending on the Fermi level, other charge states of the divacancy are stable as well [20]. In fact, the divacancy naturally exists in a dark charge state for which a ZPL cannot be measured [23]. This dark charge state, however, can be converted to the bright, neutral state through optical excitation resulting in a greatly increased photoluminescence intensity [24-26]. Different mechanisms of charge state conversion have been proposed involving either the positive charge state [26] or the negative charge state [24, 25] of the divacancy. Since the experimental evidence is not sufficient to determine the charge of the dark state with certainty, computational results were utilized to assess the proposed mechanisms. Golter et al. [26] used single particle states of the neutral defect as determined by density functional theory (DFT). They hypothesized a shift of the a_1 level of the minority spin states into the valence band upon ionization to explain the recovery of the neutral state as well as to rationalize loss of ZPL intensity. Wolfowicz et al. [25] and Magnusson et al. [24] used, instead, charge transition levels calculated from defect formation energies of the corresponding charge states to explain the electronic transitions. In both cases, the supporting computational results can be regarded as estimates of the electronic transitions involved. While DFT orbital energies, particularly for unoccupied states are unreliable, inaccuracies were introduced in [24, 25] by mixing of total energy differences (transition levels) with experimental results or single particle energies (onset of conduction band). Further, the calculation of transition levels suffers from inconsistent treatment of long range Coulomb interactions for different charge states that is only partially corrected for when using charge correction schemes [27, 28]. We have observed unsystematic errors in the charge transition levels of 0.2 eV [29]. Here, we utilize constrained DFT to calculate electronic excitation energies directly and consistently within the same charge state.

The majority of prior computational work on defects in 4H-SiC has concentrated on ground state properties. In particular, the calculation of hyperfine tensors enables comparison between computational and electron paramagnetic resonance results facilitating experimental assignment [17-19, 30-34]. Defect formation energies as a function of the Fermi level have been

computed [20, 30, 34-38] to determine charge state stabilities and transition levels. Evaluation of excited states for defects in 4H-SiC have been focused on first excited states and corresponding ZPLs, which have been calculated for the NV center [12, 20, 39, 40] and for the neutral divacancy defect using constrained DFT [12, 39, 41]. The excitation spectrum of the neutral divacancy has also been studied with time-dependent DFT [42], albeit within a finite cluster approximation.

The main objective of our work is to calculate energy requirements for conversion of the neutral divacancy defect in 4H-SiC to either the positive or the negative charge state and for corresponding recovery to the neutral charge state in order to differentiate between proposed mechanisms of optical charge state switching [25, 26]. Note that in other work [24], the capture of electrons photo-ionized from other defects was proposed to be responsible for the conversion of the neutral divacancy. This alternative scenario is not investigated herein. We also consider the defect formation energy as a function of the Fermi level to obtain information on the likelihood of charge state realization. Energy shifts of the localized defect levels during excitation are used to explain the absence of photoluminescence intensity in the dark state. While most of the computational evidence points towards the positive charge state as being involved in the mechanism of charge state switching, formation of the positive charge state without further assistance of states originating from impurities other than the divacancy is a complicated process including multiple excitations.

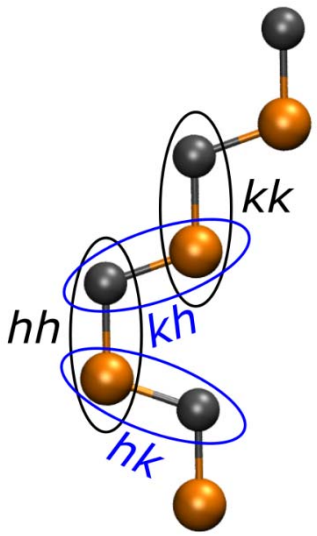

Figure 1. Atoms of the 4H-SiC unit cell showing the *hh*, *kk*, *hk*, and *kh* divacancy defect configurations; carbon – grey, silicon – orange.

2. Computational Methods

All electronic structure calculations are performed using the projector-augmented wave (PAW) method [43, 44] as implemented in the Vienna ab initio simulation package (VASP) [45-48]. Density functional theory (DFT) calculations are carried out using the Perdew-Burke-Ernzerhof (PBE) functional [49], PBE with the Grimme D3 dispersion correction (PBED) [50], and the Heyd-Scuseria-Ernzerhof (HSE), specifically the HSE06, functional [51]. We employ spin-polarized functionals and an energy cutoff of 400 eV. The nature of the defect states; i.e. localized or bulk, is determined through visualization of the PARCHG files computed with VASP.

Cell expansions are derived from the 8 atom hexagonal unit cell for bulk 4H-SiC with ABCB stacking. There are two non-equivalent lattice positions for Si and C, hexagonal *h* and cubic *k*, leading to four distinct atom combinations that are removed to form the divacancy defects and are shown in **Figure 1**. In this work, we study the *hh* defect as the representative for the two axial defects (*hh* and *kk*) and the *kh* defects as the representative for the two basal defects (*kh* and *hk*). We use the convention that the first letter denotes the position of the Si vacancy and the second letter the position of the C vacancy, consistent with the assignments of PL1 to the *hh* and PL4 to the *kh* defect [24, 26, 39, 41]. Note, however, that in recent work [52], PL4 has been assigned to the *hk* defect. We find only small differences between the two defects studied and, generally, the main text contains results for the *hh* defect, while the **Supporting Information** [53] contains corresponding values for the *hk* defect.

We use a 551 cell expansion and a Γ-centered 2-2-2 Monkhorst-Pack k-point mesh for the calculation of defect formation energies based on our previous work [29], where we have shown that a 551 cell expansion yields an error due to finite cell size effects below 0.05 eV for formation energies of the neutral divacancy using the PBE functional. Lattice parameters and ionic positions of the ground states for the *hh* and *kh* divacancy defects are optimized in their

respective charge states. Energies are obtained for defects in their most stable spin states, which is the triplet state for the neutral, the doublet state for the +1 and -1 charge states, and the singlet state for the -2 and +2 charge states. Defect formation energies are calculated as

$$E_f = E_d - E_b + \mu_C^0 + \mu_{Si}^0 + \Delta H_f + q(E_{Fermi} + VBM) + E^c, \quad (1)$$

where E_d is the defect energy, E_b the bulk energy, μ_C^0 the chemical potential of carbon, μ_{Si}^0 the chemical potential of silicon, q the charge state of the defect, E_{Fermi} the Fermi energy, and VBM the valence band maximum of the bulk. The enthalpy of formation of SiC, ΔH_f, is added assuming a carbon-rich environment. We use the code sxdefectalign [27, 28] to compute E^C. The energy term E^C corrects for interactions of periodically repeated charged defects and the interaction of the defect with the uniform background charge that is introduced in calculations of charged systems. To obtain E_d and E_b consistently in **Equation 1**, the bulk lattice and ionic positions are optimized using the same cell expansion and k-point mesh as for the defect calculation.

We use the constrained DFT formalism to compute excited state geometries and energies. Although we have previously investigated the convergence of the ZPLs with computational cell size [29], we had pointed out that the analysis may be skewed by the limitation of the Quantum Espresso implementation of constrained DFT that allows for Γ point calculations only. VASP permits the use of larger k-point meshes in combination with constrained DFT. In **Supporting Information, Figure S1** [53], we compare the convergence behavior of the ZPL with respect to computational cell size between Γ-point calculations and calculations using an extended k-point grid. The sensitivity of the ZPL to k-point sampling has also recently been shown in other work [52]. According to our results for the ZPL, we choose a 551 cell expansion (a = 15.4 □) in combination with a Γ-centered 2-2-2 Monkhorst-Pack k-point mesh to compute excitation energies. Our value for the ZPL for the *hh* defect of 0.91 eV (PBE) is very close to the reportedly converged ZPL with respect to cell size and k-point sampling [52]. However, constrained HSE geometry optimizations are prohibitively expensive on our computational resources when employing a 2-2-2 k-point mesh. We, therefore, use a 771 cell expansion (a = 21.6 □) with Γ-point sampling to investigate structural relaxation effects computed with the HSE functional. We conclude in the **Supporting Information** [53] that constrained HSE single point calculations of

PBE optimized geometries for a 551 cell expansion and a 2-2-2 k-point mesh are an appropriate choice and reported throughout the text.

In contrast to the negative charge state formation, the creation of the positive charge state involves the calculation of many highly excited states that do not converge using constrained HSE. However, we are able to obtain all desired excited states with the PBE and PBED functionals. Note, that, if the band gap is estimated as an orbital energy difference neglecting orbital relaxation, it is, with a value of 2.30 eV, severely underestimated by the PBE functional, while the HSE functional predicts a band gap of 3.24 eV, which is close to the experimental value of 3.23 eV [16]. The underestimation of the band gap with PBE potentially leads to large errors considering that the excitations of interest occur within the band gap, some involving the band edges. Nonetheless, we have calculated a ZPL for the *hh* defect using PBED that was close to the experimental value [29], although, as we have pointed out, this might have been the result of fortuitous error cancellation. We report PBED excitation energies in the **Supporting Information, Figures S3-S6** [53] when exploring all possible ionization pathways leading to the positive charge state. We apply corrections to the constrained PBE values that yield our best estimates for constrained HSE excitation energies involved in positive charge state formation. The corrections are rationalized based on comparisons of orbital energies between PBE and HSE, which is explained in detail in the **Supporting Information** [53].

We would like to point out that constrained DFT is, in principle, not well suited to describe degenerate excited states. Like DFT for the ground state, constrained DFT is a single determinant approach and we expect degraded performance when degenerate or near degenerate defect states are partially occupied. It was estimated [52] that the achievable accuracy for the ZPL of the divacancy in 4H-SiC with constrained DFT does not exceed 0.1 eV due to the multi-reference character of the wavefunction when the empty *e* states of the defect are partially occupied. Nevertheless, comparison to experimental values shows good agreement with the ZPL computed with the HSE functional for the divacancy defects in 4H-SiC [12, 39, 41].

Throughout the text, excitations are identified and visualized by their initial and final orbitals of the corresponding ground state. However, reported excitation energies are computed with constrained DFT that should not be confused with orbital energy difference calculations.

3. Results and Discussion

Positive Charge State Formation

In the single-photon pathway of positive charge state formation, an electron of majority spin is promoted from the highest occupied orbital of the ground state to the conduction band, which is visualized in **Figure 2**, $VV^0 \rightarrow VV^+$. If dissipation of the electron in the conduction band is fast compared to emission, this excitation yields the positive charge state. Excitations are depicted in **Figure 2** using a green arrow from the initial to the final HSE orbital in the corresponding ground state of the *hh* defect. The occupation of those orbitals is kept fixed during constrained HSE calculations. Ground state orbital energies of the neutral, positive, and negative charge states are drawn to scale for the Γ point (arbitrary choice, orbital energies depend on the k-point). Bulk states are very close in energy and are illustrated with continuous blocks labeled conduction and valence band. Localized defect states of the majority spin channel are drawn on the left in each pictogram and defect states of the minority spin channel on the right. If the defect state is submerged into the valence band, its energy is difficult to distinguish from the bulk energy levels. The electron is then pictured as a dashed blue half-arrow without corresponding energy level.

The calculated adiabatic excitation energy for the single-photon excitation to form the positive charge state, $VV^0 \rightarrow VV^+$, for the *hh* divacancy defect is 2.3 eV (constrained HSE). The corresponding value for the *hk* defect is given in the **Supporting Information, Table S1** [53]. This is much above the observed energy range of 1.1 to 1.3 eV [25, 26] for dark state formation. However, it is in line with the observation that ionization and conversion of the neutral divacancy defect into a dark state occurs at low rate compared to the reverse process of bright

state recovery. This led to the conclusion that multiple photons are involved in dark state creation [25, 26]. The computed single-photon excitation energy provides a minimum value at which a single-photon process can contribute. If the dark state is the positive charge state, a rate increase of dark state formation should be observable above 2.3 eV indicating a switch from a multi-photon to a single-photon mechanism.

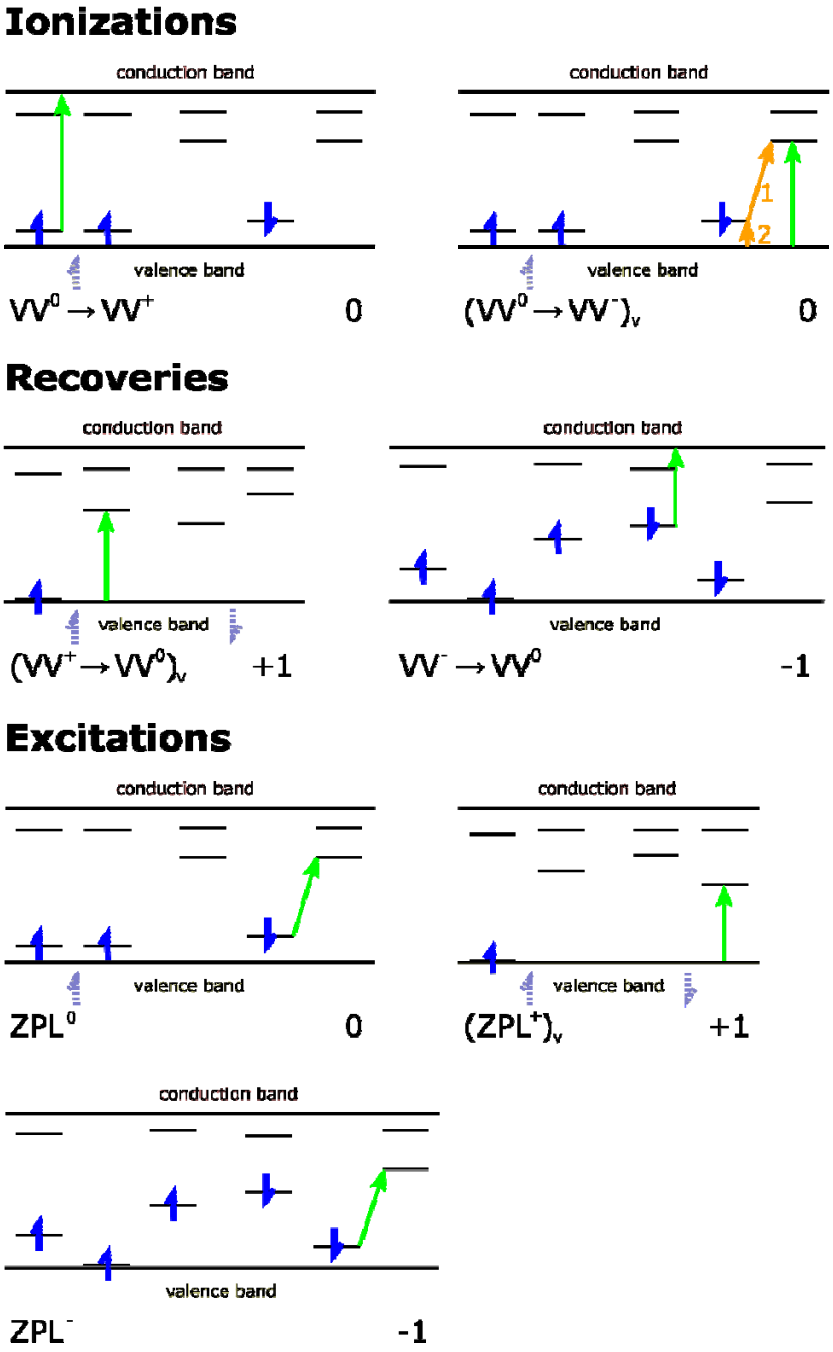

Figure 2. Visualization of excitations (green arrows) indicating initial and final orbitals that are kept fixed during constrained DFT for majority (upward blue arrows) and minority (downward blue arrows) spin channels, HSE orbital energies of the *hh* ground states are drawn to scale at the Γ point, type of excitation and charge of the ground state are marked below the pictograms, subscript v indicates excitation from highest valence band, orange arrows show the stepwise conversion from neutral to negative charge state.

Due to convergence problems when applying constrained HSE (see **Computational Methods**), we compute excitation energies of multi-photon processes leading to positive charge state formation with constrained PBED. The **Supporting Information, Figures S3-S6** [53] contain all possible stepwise excitations that lead to placement of a majority spin electron from the lowest defect state into the conduction band for the *hh* and *hk* defects. We conclude in the **Supporting Information** [53] that it is unlikely that any of the multi-photon ionization pathways directly lead to ionization. However, following a similar argument as in Golter et al. [26], the spontaneous deexcitation of a minority spin electron from a higher excited state may provide the energy for a simultaneous excitation of a majority spin electron. Note, however, that in Golter et al. [26], it was assumed that the upper defect *e* states shift into the conduction band after initial excitation corresponding to the ZPL of the neutral defect. In contrast, we find that the upper quasi-degenerate majority spin defect states in the first excited state are more than 0.4 eV below the conduction band (computed with HSE). Occupation of the defect states will lower their energy further into the gap requiring an additional excitation step. A modified, potential excitation path is shown in **Figure 3** with corresponding adiabatic excitation energies for the *hh* defect given in **Table 1** (PBED adiabatic). Results for the *hk* defect are included in the **Supporting Information, Table S3** [53]. The first two steps constitute a 2-photon process, where the experimentally observed first excitation (ZPL) of the minority spin electron is followed by a second excitation into the upper minority spin defect levels. Spontaneous deexcitation from E_2 provides the energy to promote a majority spin electron into the empty majority defect states. Excitation of that electron into the conduction band completes the path of positive charge state formation assuming fast dissipation of the electron in the conduction band.

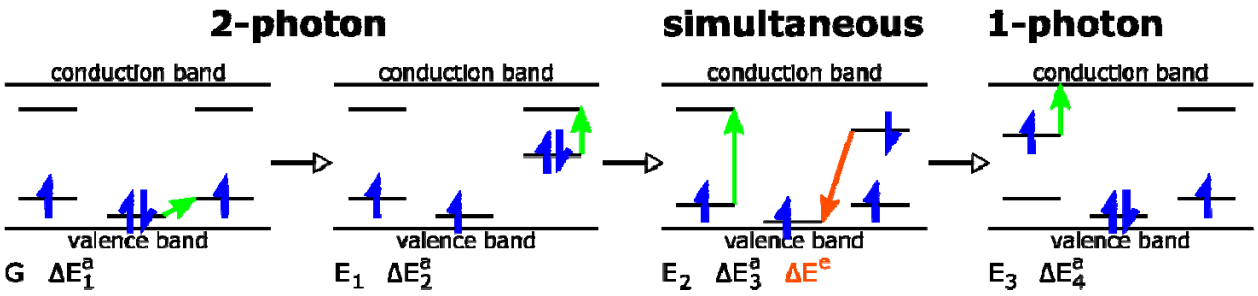

Figure 3. Potential pathway of positive charge state creation from the neutral divacancy defect in 4H-SiC; upward blue arrows indicate majority and downward blue arrows minority spin electrons, green arrows denote electronic excitations from schematically shown initial states in ground (G), first excited (E_1), second excited (E_2), and third excited (E_3) states, orange arrow visualizes emission; energy differences ΔE correspond to arrows with energies given in **Table 1**; for simplicity energy levels of majority and minority spin states are not distinct.

Excitation	PBED adiabatic	PBED vertical	best estimate
Δ	0.95	1.03[i]	1.21
Δ	0.71	1.04[ii]	1.04
Δ	1.26	1.48[ii]	1.68
Δ	0.82	1.15[iii]	1.15
Δ	1.66	1.60[ii]	1.80

Table 1. Adiabatic, vertical excitation energies (ΔE^a) and emission energy (ΔE^e) in eV corresponding to the pathway shown in **Figure 3** and calculated with constrained PBED for the *hh* divacancy defect in 4H-SiC, best estimates for excitation energies defined in text; [i] ground state, [ii] E_1, [iii] E_3 geometries are used.

However, while measured ZPLs are adiabatic excitation energies, observed limiting energy requirements for charge state conversion correspond to vertical excitation energies. We, therefore, determine vertical excitation energies for likely initial and final state geometries during absorption and emission that may lead to an energetically attainable pathway of positive charge state formation corresponding to **Figure 3** (PBED vertical in **Table 1** for the *hh* defect and in **Supporting Information, Table S3** [53] for the *hk* defect). For absorption ΔE_1^a, initial and final geometries are that of the ground state. The first excited state (E_1) is assumed to have a long enough life time for structural relaxation to occur as evident by the measurable ZPL. To that effect, the vertical ΔE_2^a is calculated using the geometry of the E_1 excited state. The resulting higher excited state E_2, however, may be short lived. In fact, vertical deexcitation from E_2 results in an emission energy of 1.31 eV for the *hh* defect and is likely not sufficient to cause excitation of the majority spin electron (ΔE_3^a). For the calculation of ΔE^e and ΔE_3^a we, therefore, use the geometry of the E_1 state, in line with a short lived E_2. Excited state E_3 has to exist long enough for further promotion of the electron into the conduction band (ΔE_4^a). To that end, we use the geometry of the E_3 state to compute the vertical excitation ΔE_4^a.

Next, we apply the reasoning explained in the **Supporting Information** [53] to obtain best estimates for constrained HSE excitation energies, which are given in **Table 1** for the *hh* defect and discussed in the following. **Supporting Information, Table S3** [53] contains corresponding estimates for the *hk* defect. According to our best estimates, the mechanism of positive charge state formation according to **Figure 3** is energetically feasible, albeit occurring with potentially very low intensity due to the participation of multiple-photon processes. 2-photon excitation of a minority spin electron requires an energy of 1.26 eV, which is close to the experimentally observed limit of 1.1 eV [25, 26]. Assuming a short life time of E_2, deexcitation of the minority spin electron releases sufficient energy (1.80 eV) for the simultaneous excitation of the majority spin electron into the unoccupied defect states (absorption energy of 1.68 eV) located within the band gap. Further promotion of the majority spin electron into the conduction band with an absorption energy of 1.15 eV accompanied by fast electron dissipation into the bulk may be responsible for dark charge state formation. A similar assessment can be made for the *hk* defect, see **Supporting Information, Table S3** [53]. Although a low charge state conversion rate has

been observed experimentally [26], verification of the identified pathway of positive charge state formation involving multiple-photon processes is highly desirable.

Negative Charge State Formation

Formation of the negative charge state is far less complicated, although it also requires 2-photon absorption. This is because the promotion of an electron from the valence band into the quasi-degenerate minority defect state, which is visualized in **Figure 2**, $(VV^0 \rightarrow VV^-)_v$ by a green arrow, consumes an energy of more than 2 eV. As indicated with orange arrows in **Figure 2**, the negative charge state may, instead, be formed through 2-photon excitation. The first excited state E_1 (orange arrow 1) is obtained with an adiabatic excitation energy of 1.13 eV (ΔE(HSE) for ZPL^0 in **Supporting Information, Table S1** [53], *hh* defect) followed by a promotion of an electron from the valence band into the lowest unoccupied orbital of the E_1 excited state (orange arrow 2). While we did not obtain an HSE result for the second excitation, its adiabatic excitation energy is given as the difference between the adiabatic excitation energy for $(VV^0 \rightarrow VV^-)_v$ and ZPL^0, which is 0.96 eV for the *hh* defect. Adding relaxation terms obtained from the difference of vertical and adiabatic excitation energies computed with constrained PBED yields consecutive absorption energies of 1.21 eV and 1.11 eV for the *hh* defect (1.27 eV and 1.05 eV for the *hk* defect, respectively).

Our results suggest that the energy requirements to form the positive and the negative charge state from the neutral divacancy defect are very similar with a calculated minimum energy between 1.2 and 1.3 eV. Both charge states are formed involving a 2-photon excitation. However, the mechanism of positive charge state creation constitutes a series of processes. If at all, we expect a lower rate of charge state conversion for the positive charge state.

Neutral Defect Recovery

While conversion of the neutral defect into the dark charge state reduces photoluminescence intensity, a strong enhancement of the signal was observed when the pump laser energy reached about 1.3 eV [25, 26]. This was explained by the conversion of the naturally dark state of the divacancy into the neutral state [23, 25, 26]. The recovery of the bright state from the positive and the negative charge state are visualized in **Figure 2**, $(VV^+ \rightarrow VV^0)_v$ and $VV^- \rightarrow VV^0$. The corresponding adiabatic excitation energies for the *hh* defect obtained with constrained HSE are 1.36 and 1.49 eV, respectively. The calculated vertical excitation energies for either the positive defect, with a value of 1.47 eV, or the negative defect, with a value of 1.68 eV, are above the experimentally observed minimum energy at which enhancement occurs. Similarly for the *hk* defect, see **Supporting Information, Table S4** [53].

Recalling the analysis of our computational results that led to the corrections of constrained PBE results to obtain best estimates for constrained HSE values and that is detailed in the **Supporting Information** [53], we notice a large difference between PBE and HSE ground state orbital energies for orbitals involved in the $(VV^+ \rightarrow VV^0)_v$ excitation. This manifests itself in large constrained HSE values compared to constrained PBED results and might point to a source of error. For $VV^- \rightarrow VV^0$, the difference between constrained HSE and constrained PBED excitation energies is moderate. In addition, there is a fairly large difference between the constrained PBE results for the 551 and the 771 cell expansion for both, the $(VV^+ \rightarrow VV^0)_v$ and the $VV^- \rightarrow VV^0$ excitation (see **Supporting Information, Table S1** [53]), suggesting that the computational cell size is not quite converged for the charged defects. However, the computed energy requirement for neutral state recovery from the positive charge state, with a value of 1.47 eV, fits the experimental value of 1.3 eV [25, 26] better than from the negative charge state, with a value of 1.68 eV.

Zero Phonon Lines

In **Figure 2**, the excitation leading to the experimentally observed ZPL in the neutral charge state (ZPL^0) is depicted together with the corresponding excitations in the positive (ZPL^+) and the negative (ZPL^-) charge states. In the positive charge state, the defect state from which the

excitation originates is shifted into the valence band. If the electron hole that is created in the valence band during excitation, dissipates fast enough compared to emission, there is no electronic state available for the excited electron to fall back to. This suggests, in line with the arguments presented in previous work [26], that the positive charge state is indeed dark. However, since emission occurs from the excited state, we analyze the orbital energies of the excited state that corresponds to ZPL^{+}. The orbital energy of the now unoccupied defect state lies less than 0.1 eV above the valence band. An energy difference of 0.1 eV is within the expected error margin for occupied defect state energy differences using a 551 cell expansion [29]. If the unoccupied defect state is indeed situated above the valence band, this may slow electron hole dissipation. However, with a variational energy optimization procedure, unoccupied orbital energies are determined with much less accuracy than occupied orbital energies since they do not contribute to the total energy change of the system. Given the large uncertainty in unoccupied state energies in combination with the small energy difference of the unoccupied state to the valence band, we support the previously made argument [26] that the positive charge state may appear dark in photoluminescence experiments due to the repopulation of the defect state with bulk electrons.

In contrast, the originating defect state of the excitation corresponding to the observed ZPL in the negative charge state (ZPL^{-}) is well within the band gap, as illustrated in **Figure 2**. In the excited state, the energy of the unoccupied defect state that has been created during excitation, increases further and is situated more than 0.9 eV above the valence band. Deexcitation to form the ground state of the negative defect does not appear to be hindered and there is no computational evidence that the negative charge state is dark.

Defect Formation Energies

Finally, we consider defect formation energies to obtain insight into the stability of the charge states as a function of the Fermi level. The defect formation energy plot calculated with the HSE functional for the *hh* defect can be found in **Figure 4**, for the *hk* defect in **Supporting Information, Figure S7** [53]. The corresponding plots computed with the PBE functional are

contained in the **Supporting Information, Figure S8** [53]. Results for the *hh* and the *hk* defect are again comparable. While the overall shape of the curves calculated with the PBE and the HSE functional is similar, the location of the charge transition levels depends on the density functional and the charge correction scheme employed [35, 36, 40, 41]. As observed previously [35], the defect formation energy of the neutral relative to the charged defects is predicted to be larger with the HSE functional than with the PBE functional. This results in an increased stability range of the positive charge state when the presumably more accurate HSE functional is used. In contrast, the stability range of the negative charge state has been calculated to be small [36, 40, 41]. Focusing on the HSE results, we compute a Fermi energy range of 1.27 eV for the positive charge state of the *hh* defect (1.20 eV for *hk*) and only 0.14 eV for the negative charge state of the *hh* defect (0.17 eV for *hk*). It is, therefore, unlikely that the naturally existing charge state is the negative charge state. If that was the case, we would expect a strong dependence of the conversion mechanism on sample origin and preparation, since small changes in impurity concentration may shift the Fermi level and, correspondingly, the relative stability of the defect charge states. However, charge state conversion was consistently seen in experiment [24-26]. In contrast, moderate changes in sample preparation should not affect the mechanism of charge state conversion if the observed dark state is the positive charge state since it exists in a wide range of Fermi energy.

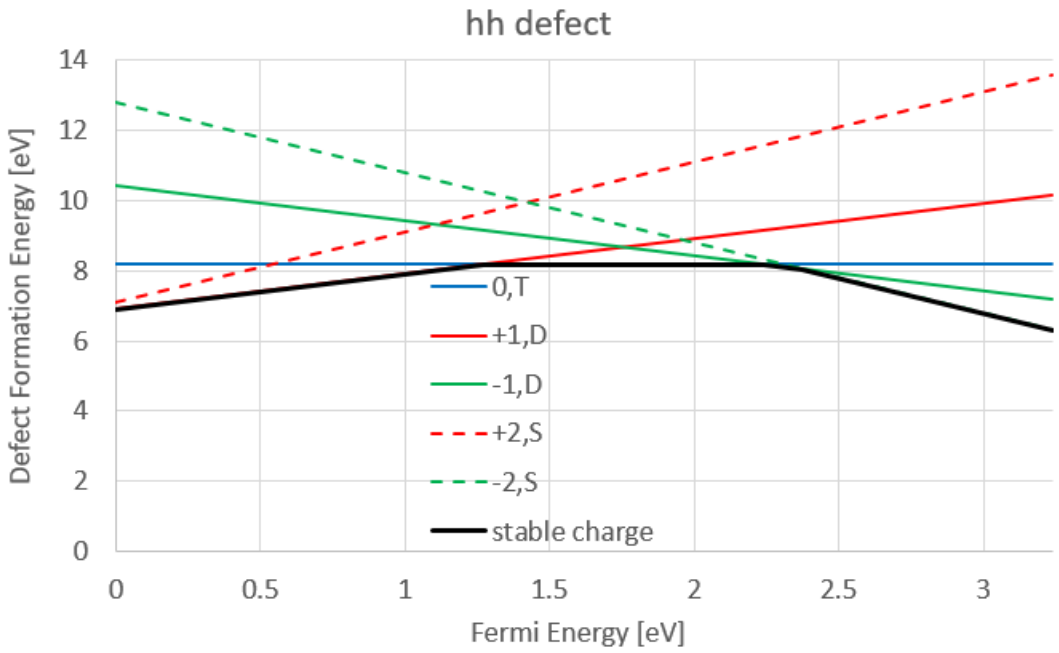

Figure 4. Defect formation energy as a function of the Fermi energy sweeping through the band gap (3.24 eV) computed with HSE for the neutral triplet (0, T), positive doublet (+1, D), negative doublet (-1, D), doubly positive singlet (+2, S), doubly negative singlet (-2, S), and most stable charge state of the *hh* divacancy defect in 4H-SiC

4. Conclusions

We have used constrained DFT to investigate the mechanism of charge state conversion from the bright neutral charge state of the divacancy defect in 4H-SiC to a dark state observed in photoluminescence experiments [24-26]. We focused on the *hh* and *hk* defects. We considered multi-photon excitation yielding the positive [26] and the negative charge states [25] as well as corresponding recovery of the neutral charge state. Notably, we did not investigate ionization mechanisms that rely on neighboring defects [24] nor did we study doubly charged states.

We calculated zero phonon lines (ZPLs) of the neutral divacancy and the corresponding excitations for the positive and negative charge states. Due to the shift of the highest occupied

defect state of the minority spin channel into the valence band in the ground state of the positive charge state, which is maintained (within 0.1 eV) in the excited state, the positive charge state is confirmed to be dark. This assumes fast hole dissipation in the valence band. In contrast, we do not find evidence that the negative charge state is dark since the defect states involved in the lowest excitation of the minority spin electron are well within the band gap and a corresponding ZPL should be observable.

We identified a possible pathway of positive charge state formation involving a 2-photon excitation of the minority spin electron followed by simultaneous deexcitation and excitation of the majority spin electron. The excited majority spin electron is then further promoted into the conduction band creating the positive charge state assuming fast dissipation of the electron in the conduction band compared to emission. The negative charge state formation only requires a 2-photon process and may proceed at higher rate. However, if the negative charge state is bright (a ZPL is detectable), experimentally observed signal changes cannot be explained utilizing the negative charge state. The computed absorption energies, determining the minimum energy required for charge state formation, are 1.2 eV for either the positive or the negative charge state, comparing well to the observed threshold of 1.1 eV [25, 26].

Our computational results overestimate the observed minimum energy of 1.3 eV required for neutral charge state recovery [25, 26] for both charged states. The neutral charge state is recovered from the positive charge state by excitation of an electron from the valence band into the unoccupied majority spin defect state, again assuming fast hole dissipation. The corresponding absorption energy is computed to be 1.5 eV. The neutral charge state is recovered from the negative charge state by the excitation of a minority spin electron into the conduction band followed by dissipation of the electron into the bulk. The required absorption energy is calculated to be 1.7 eV. The overestimation of the absorption energies may be due to a less well converged computational cell size for excitations in charged compared to neutral defects.

Further, we computed defect formation energies as a function of the Fermi level. We observed that the negative charge state is most stable in a very narrow Fermi energy range, while the positive charge state is most stable in a wide stability range. If the negative charge state was the dark charge state, we would expect a high sensitivity of the mechanism of charge state

conversion to sample preparation due to differing impurity concentration and corresponding Fermi level shifts, which was not reported.

In summary, we have collected computational evidence supporting the identification of the dark charge state as the positive charge state in the mechanism of optical charge state switching. In our opinion, it is less likely that the negative charge state is the dark charge state. However, the identified pathway of positive charge state formation involves a series of excitation processes. Further research into positive charge state creation of the divacancy is warranted.

Acknowledgement

This work was funded by the Department of Defense and conducted at the US Army Research Laboratory. It was supported in part by a grant of computer time from the DOD High Performance Computing Modernization Program at the ARL, Navy, AFRL and ERDC DoD Supercomputing Resource Centers. AB was sponsored by the Army Research Laboratory under Cooperative Agreement Number W911NF-17-2-0040. The views and conclusions contained in this document are those of the authors and should not be interpreted as representing the official policies, either expressed or implied, of the Army Research Laboratory or the U.S. Government. The U.S. Government is authorized to reproduce and distribute reprints for Government purposes notwithstanding any copyright notation herein.

References

1. X. Shi, L. F. Wei, and C. H. Oh, Quantum computation with surface-state electrons by rapid population passages, Science China-Physics Mechanics & Astronomy 57, 1718 (2014).
2. P. M. Platzman and M. I. Dykman, Quantum computing with electrons floating on liquid helium, Science, 284, 1967 (1999).
3. D. G. Cory, R. Laflamme, E. Knill, L. Viola, T. F. Havel, N. Boulant, G. Boutis, E. Fortunato, S. Lloyd, R. Martinez, C. Negrevergne, M. Pravia, Y. Sharf, G. Teklemariam, Y. S. Weinstein, and W. H. Zurek, NMR based quantum information processing: Achievements and prospects, Fortschritte Der Physik-Progress of Physics 48, 875 (2000).

4. L. Wang, T. Tu, B. Gong, and G. C. Guo, Decoherence-protected spin-photon quantum gates in a hybrid semiconductor-superconductor circuit, Physical Review A 92, 062346 (2015).
5. F. Hassler, G. Catelani, and H. Bluhm, Exchange interaction of two spin qubits mediated by a superconductor, Physical Review B 92, 235401 (2015).
6. A. Walther, L. Rippe, Y. Yan, J. Karlsson, D. Serrano, A. N. Nilsson, S. Bengtsson, and S. Kroll, High-fidelity readout scheme for rare-earth solid-state quantum computing, Physical Review A 92, 022319 (2015).
7. D. Serrano, Y. Yan, J. Karlsson, L. Rippe, A. Walther, S. Kroll, A. Ferrier, and P. Goldner, Impact of the ion-ion energy transfer on quantum computing schemes in rare-earth doped solids, Journal of Luminescence 151, 93 (2014).
8. S. Debnath, N. M. Linke, C. Figgatt, K. A. Landsman, K. Wright, and C. Monroe, Demonstration of a small programmable quantum computer with atomic qubits, Nature 536, 63 (2016).
9. N. A. Sobolev, Y. V. Vyzhigin, B. N. Gresserov, E. I. Sheck, A. I. Kurbakov, E. E. Rubinova, and V. A. Trunov, Silicon Device Engineering by Intrinsic Point-Defect Control, Gettering and Defect Engineering in Semiconductor Technology 19, 169 (1991).
10. J. I. Nishizawa, Stoichiometry control and point defects in compound semiconductors, Materials Science in Semiconductor Processing 6, 249 (2003).
11. L. Gordon, J. R. Weber, J. B. Varley, A. Janotti, D. D. Awschalom, and C. G. Van de Walle, Quantum computing with defects, Mrs Bulletin 38, 802 (2013).
12. J. R. Weber, W. F. Koehl, J. B. Varley, A. Janotti, B. B. Buckley, C. G. Van de Walle, and D. D. Awschalom, Quantum computing with defects, Proceedings of the National Academy of Sciences of the United States of America 107, 8513 (2010).
13. L. Childress, M. V. G. Dutt, J. M. Taylor, A. S. Zibrov, F. Jelezko, J. Wrachtrup, P. R. Hemmer, and M. D. Lukin, Coherent dynamics of coupled electron and nuclear spin qubits in diamond, Science 314, 281 (2006).
14. P. Neumann, N. Mizuochi, F. Rempp, P. Hemmer, H. Watanabe, S. Yamasaki, V. Jacques, T. Gaebel, F. Jelezko, and J. Wrachtrup, Multipartite entanglement among single spins in diamond, Science 320, 1326 (2008).
15. M. V. G. Dutt, L. Childress, L. Jiang, E. Togan, J. Maze, F. Jelezko, A. S> Zibrov, P. R. Hemmer, and M. D. Lukin, Quantum register based on individual electronic and nuclear spin qubits in diamond, Science 316, 1312 (2007).
16. Y. Goldberg, M. E. Levinshtein, and S. L. Rumyantsev, in Properties of Advanced Semiconductor Materials GaN, AlN, SiC, BN, SiC, SiGe, M. E. Levinshtein, S. L. Rumyantsev, and M. S. Shur, Editors. 2001, John Wiley & Sons: New York. p. 93 - 148.
17. J. Isoya, T. Umeda, N. Mizuochi, N. T. Son, E. Janzen, and T. Ohshima, EPR identification of intrinsic defects in SiC, Physica Status Solidi B-Basic Solid State Physics 245, 1298 (2008).
18. H. J. von Bardeleben, J. L. Cantin, A. Csore, A. Gali, E. Rauls, and U. Gerstmann, NV centers in 3C, 4H, and 6H silicon carbide: A variable platform for solid-state qubits and nanosensors, Physical Review B 94, 121202(R) (2016).
19. T. Umeda, J. Ishoya, T. Ohshima, N. Morishita, H. Itoh, and A. Gali, Identification of positively charged carbon antisite-vacancy pairs in 4H-SiC, Physical Review B 75, 245202 (2007).
20. J. R. Weber, W. F. Koehl, J. B. Varley, A. Janotti, B. B. Buckley, C. G. Van de Walle, and D. D. Awschalom , Defects in SiC for quantum computing, Journal of Applied Physics 109, 102417 (2011).
21. D. J. Christle, A. L. Falk, P. Andrich, P. V. Klimov, J. Ul Hassan, N. T. Son, E. Janzen, T. Ohshima, and D. D. Awschalom, Isolated electron spins in silicon carbide with millisecond coherence times, Nature Materials 14, 160 (2015).

22. W. F. Koehl, B. B. Buckley, F. J. Heremans, G. Calusine, and D. D. Awschalom, Room temperature coherent control of defect spin qubits in silicon carbide, Nature 479, 84 (2011).
23. C. F. de las Casas, D. J. Christle, J. U, Hassan, T. Ohshima, N. T. Son, and D. D. Awschalom, Stark tuning and electrical charge state control of single divacancies in silicon carbide, Applied Physics Letters 111, 262403 (2017).
24. B. Magnusson, N. T. Son, A. Csore, A. Gallstrom, T. Ohshima, A. Gali, and I. G. Ivanov, Excitation properties of the divacancy in 4H-SiC, Cornell University Library (2018) (https://arxiv.org/abs/1804.01167).
25. G. Wolfowicz, C. P. Anderson, A. Yeats, S. J. Whiteley, J. Niklas, O. Poluektov, F. J. Heremans, and D. D. Awschalom, Optical charge state control of spin defects in 4H-SiC, Nature Communications 8, 1876 (2017).
26. D. A. Golter, and C. W. Lai, Optical switching of defect charge states in 4H-SiC, Scientific Reports 7, 13406 (2017).
27. C. Freysoldt, J. Neugebauer, and C. G. Van de Walle, Fully Ab Initio Finite-Size Corrections for Charged-Defect Supercell Calculations, Physical Review Letters 102, 016402 (2009).
28. C. Freysoldt, J. Neugebauer, and C. G. Van de Walle, Electrostatic interactions between charged defects in supercells, Physica Status Solidi B-Basic Solid State Physics 248, 1067 (2011).
29. A. Beste and D. E. Taylor, Convergence of Ground and Excited State Properties of Divacancy Defects in 4H-SiC with Computational Cell Size, US Army Research Laboratory, ARL-TR-8313 (2018).
30. P. Carlsson, N. T. Son, A. Gali, J. Isoya, N. Morishita, T. Ohshima, B. Magnusson, and E. Janzen, EPR and ab initio calculation study on the EI4 center in 4H- and 6H-SiC, Physical Review B 82, 235203 (2010).
31. T. Umeda, Y. Ishitsuka, J. Isoya, N. T. Son, E. Janzen, N. Morishita, T. Ohshima, H. Itoh, and A. Gali, EPR and theoretical studies of negatively charged carbon vacancy in 4H-SiC, Physical Review B 71, 193202 (2005).
32. M. Bockstedte, M. Heid, and O. Pankratov, Signature of intrinsic defects in SiC: Ab initio calculations of hyperfine tensors, Physical Review B 67, 193102 (2003).
33. N. T. Son, P. Carlsson, J. Ul Hassan, E. Janzen, T. Umeda, J. Isoya, A. Gali, M. Bockstedte, M. Morishita, T. Ohshima, and H. Itoh, Divacancy in 4H-SiC, Physical Review Letters 96, 055501 (2006).
34. X. T. Trinh, K. Szasz, T. Hornos, K. Kawahara, J. Suda, T. Kimoto, A. Gali, E. Janzen, and N. T. Son, Negative-U carbon vacancy in 4H-SiC: Assessment of charge correction schemes and identification of the negative carbon vacancy at the quasicubic site, Physical Review B 88, 235209 (2013).
35. J. I. Iwata, C. Shinei, and A. Oshiyama, Density-functional study of atomic and electronic structures of multivacancies in silicon carbide, Physical Review B 93, 125202 (2016).
36. L. Torpo, T. E. M. Staab, and R. M. Nieminen, Divacancy in 3C- and 4H-SiC: An extremely stable defect, Physical Review B 65, 085202 (2002).
37. L. Torpo, M. Marlo, T. E. M. Staab, and R. M. Nieminen, Comprehensive ab initio study of properties of monovacancies and antisites in 4H-SiC, Journal of Physics-Condensed Matter 13, 6203 (2001).
38. A. Zywietz, J. Furthmuller, and F. Bechstedt, Vacancies in SiC: Influence of Jahn-Teller distortions, spin effects, and crystal structure, Physical Review B 59, 15166 (1999).
39. S. A. Zargaleh, B. Eble, S. Hameau, J. L. Cantin, L. Legrand, M. Bernard, F. Margaillan, J. S. Lauret, J. F. Roch, H. J. von Bardeleben, F. Rauls, U. Gerstmann, and F. Treussart, Evidence for near-infrared photoluminescence of nitrogen vacancy centers in 4H-SiC, Physical Review B 94, 060102(R) (2016).
40. A. Csore, H. J. von Bardeleben, J. L. Cantin, and A. Gali, Characterization and formation of NV centers in 3C, 4H, and 6H SiC: An ab initio study, Physical Review B 96, 085204 (2017).

41. L. A. Gordon, L., A. Janotti, and C. G. Van de Walle, Defects as qubits in 3C- and 4H-SiC, Physical Review B 92, 045208 (2015).
42. A. Gali, Time-dependent density functional study on the excitation spectrum of point defects in semiconductors, Physica Status Solidi B-Basic Solid State Physics 248, 1337 (2011).
43. P. E. Blochl, Projector Augmented-Wave Method, Physical Review B 50, 17953 (1994).
44. G. Kresse and D. Joubert, From ultrasoft pseudopotentials to the projector augmented-wave method, Physical Review B 59, 1758 (1999).
45. G. Kresse and J. Hafner, Abinitio Molecular-Dynamics for Liquid-Metals, Physical Review B 47, 558 (1993).
46. G. Kresse and J. Hafner, Ab-Initio Molecular-Dynamics Simulation of the Liquid-Metal Amorphous-Semiconductor Transition in Germanium, Physical Review B 49, 14251 (1994).
47. G. Kresse and J. Furthmuller, Efficiency of ab-initio total energy calculations for metals and semiconductors using a plane-wave basis set, Computational Materials Science 6, 15 (1996).
48. G. Kresse and J. Furthmuller, Efficient iterative schemes for ab initio total-energy calculations using a plane-wave basis set, Physical Review B 54, 11169 (1996).
49. J. P. Perdew, K. Burke, and M. Ernzerhof, Generalized gradient approximation made simple, Physical Review Letters 77, 3865 (1996).
50. S. Grimme, J. Antony, S. Ehrlich, H. Krieg, A consistent and accurate ab initio parametrization of density functional dispersion correction (DFT-D) for the 94 elements H-Pu, Journal of Chemical Physics 132, 154104 (2010).
51. J. Heyd, G. E. Scuseria, and M. Ernzerhof, Hybrid functionals based on a screened Coulomb potential, Journal of Chemical Physics 118, 8207 (2003).
52. J. Davidsson, V. Ivady, R. Armiento, N. T. Son, A. Gali, and I. A. Abrikosov, First principles predictions of magneto-optical data for semiconductor point defect identification: the case of divacancy defects in 4H-SiC, New Journal of Physics 20, 023035 (2018).
53. See Supplemental Material at [URL] for ZPL as a function of cell size and k-point sampling, quality assessment of constrained PBE/PBED excitation energies as compared to constrained HSE, structural relaxation effects on constrained HSE excitation energies, constrained PBED results for positive charge state formation, applied strategy to obtain best estimates for constrained HSE excitation energies for positive charge state formation, excitation energies for *hh* and *hk* defects for neutral defect recovery, defect formation energies for the *hk* defect computed with HSE, defect formation energies computed with PBE.